Organic Geochemistry 128 (2019) 86–93

Contents lists available at ScienceDirect

Organic Geochemistry

journal homepage: www.elsevier.com/locate/orggeochem

Temporal constraints on lateral organic matter transport along a coastal mud belt

Rui Bao [a,b,*,1], Meixun Zhao [c,d], Ann McNichol [b], Valier Galy [e], Cameron McIntyre [a,f,g], Negar Haghipour [a], Timothy I. Eglinton [a,e]

[a] Geological Institute, ETH Zurich, Zurich, Switzerland
[b] National Ocean Science Accelerator Mass Spectrometry Facility, Woods Hole Oceanographic Institute, Woods Hole, MA, USA
[c] Key Laboratory of Marine Chemistry Theory and Technology, Ministry of Education/Institute for Advanced Ocean Studies, Ocean University of China, Qingdao, China
[d] Laboratory for Marine Ecology and Environmental Science, Qingdao National Laboratory for Marine Science and Technology, Qingdao, China
[e] Department of Marine Chemistry and Geochemistry, Woods Hole Oceanographic Institute, Woods Hole, MA, USA
[f] Laboratory for Ion Beam Physics, ETH Zurich, Zurich, Switzerland
[g] Scottish Universities Environmental Research Centre, Glasgow, UK

ARTICLE INFO

Article history:
Received 28 September 2018
Received in revised form 1 January 2019
Accepted 16 January 2019
Available online 17 January 2019

Keywords:
East China Sea
^{14}C aging
Organic matter
Continental shelf seas
Mud belt
Sediment resuspension

ABSTRACT

Constraints on timescales of lateral transport of sedimentary organic carbon (OC) over continental shelves and associated influences on the distribution and abundance of OC remain sparse. Preferential degradation of labile, young OC during lateral transport results in apparent "diagenetic aging" of OC. Additionally, sediment translocation can also result in "transport time-associated aging" of associated organic matter (OM) as a function of the lateral transport time (LTT). Here, we use a coupled thermal decomposition and radiocarbon (^{14}C) approach to constrain timescales of lateral transport and concomitant loss of OC associated with different grain size fractions of sediments collected from two locations ~275 km apart along a dispersal pathway on the inner shelf of the East China Sea. The ^{14}C age contrasts between corresponding thermal fractions are used to distinguish these two components of sedimentary OM "aging". To minimize interferences from hydrodynamic sorting and diagenetic aging of OC accompanying lateral transport, we assess ^{14}C age differences of decomposition products from the most thermally-refractory OC components associated with specific grain size fractions between locations. We show that LTTs vary among different grain size fractions, and examine relationships between LTTs and sedimentary OC loss in order to assess the decomposition of OC as a consequence of lateral transport. We suggest that the decomposition of OC associated with protracted lateral transport exerts a strong influence on OC burial efficiency, with broad implications for carbon cycling over continental shelves.

1. Introduction

There is increasing evidence that organic carbon (OC) delivered to and produced on continental shelves can be subject to lateral advection during which it undergoes aging, further degradation and modification (Hedges et al., 1999; Inthorn et al., 2006; Tesi et al., 2016; Bao et al., 2016, 2018a; Bröder et al., 2018). A key consideration is the timescale over which organic matter (OM) is subject to these processes during lateral transport along and/or across continental shelves (Keil et al., 2004; Aller and Blair, 2004). Lateral transport of OC includes two main processes: movement of OC that is continuously maintained in suspension in the water column, and entrainment OC in resuspension-deposition loops on the sea floor (McKee et al., 1983). Keil et al. (2004) estimated that lateral transport of OC, termed transport-related oxygen exposure times ($_t$OET), might be up to 8000 years during transport across the Washington margin based on bulk OC radiocarbon (^{14}C) data of surface sediments. In a separate study, Ohkouchi et al. (2003) observed offsets of 7000 ^{14}C yr between alkenone and foraminiferal ages isolated from the same sediment layers in a deep-sea core from the Bermuda Rise, implying aging associated with lateral transport of the organic compounds prior to eventual burial. Application of the same approach to a range of other marine depositional settings has also revealed age offsets up to several millennia (Mollenhauer et al., 2005, 2011). Recently, Bröder et al (2018) argued that OM transport requires ~3600 years across the 600 km transect on the East Siberian Arctic shelf based on biomarker ^{14}C data. Bao et al.

* Corresponding author.
E-mail address: rui_bao@fas.harvard.edu (R. Bao).
[1] Present address: Department of Earth and Planetary Sciences, Harvard University, MA, USA.

https://doi.org/10.1016/j.orggeochem.2019.01.007
0146-6380/

(2018a) suggested that lateral transport of sedimentary OM ranges from hundreds to thousands of years using ^{14}C age differences of long-chain leaf wax fatty acids in specific sediment grain size fractions along two dispersal pathways of fluvially-derived material (~500 km transect along the Shandong Peninsula in the Bohai and Yellow Sea; ~35 km transect across outer shelf and upper slope on the Washington Margin, northeast Pacific Ocean).

Estimation of OC transport times along a sediment dispersal pathway based on ^{14}C measurements on bulk OC (Keil et al., 2004) carries significant uncertainty. This is because differences in measured OC ^{14}C ages between locations will reflect ^{14}C changes resulting from a combination of (1) preferential degradation of more labile (i.e., younger) OC, and resulting in enrichment in more refractory (older) OC, here termed "diagenetic aging" (Aller and Blair, 2004; Aller et al., 2008) (t_1), and (2) lateral transport time (LTT) associated radioactive decay during transport (t_2), here termed "transport time-associated aging". Interpretation of temporal offsets in bulk OC ^{14}C ages associated with across-margin transport (McCave, 2002; Keil et al., 2004) as true LTTs thus require accounting for the influence of t_1. Moreover, contribution of marine OC usually contributing younger OC along the transport pathway may reduce apparent LTTs if only calculated based on bulk OC ages.

Timescales of sediment and OC translocation depend on both the transport mechanism and associated hydrodynamic conditions. The importance of hydrodynamic processes in mobilizing and redistributing sedimentary particles has been highlighted previously (Thomsen and Gust, 2000; Thomsen and McCave, 2000). Grain size distributions of continental margin sediments vary markedly, reflecting hydrodynamic conditions and influencing the reactivity of associated OC (Thomsen and Gust, 2000; Bao et al., 2016). For instance, variable erosion thresholds and transport speeds can result in different LTTs for different grain size fractions comprising bulk sediment (Bao et al., 2018a). Moreover, because grain size is inversely related to mineral surface area (Bao et al., 2018d), and the latter is considered a primary control on OM stability (Mayer, 1994), variations in grain size may also lead to differential diagenetic aging (t_1) (Wakeham et al., 2009). ^{14}C measurements on OC associated with specific grain size fractions thus reduce potential distortions in timescales of lateral transport resulting from hydrodynamically-driven changes in grain size distribution along the transport pathway (McCave, 2002).

In this study, we employ a novel approach of ramped pyrolysis-oxidation (RPO) coupled with ^{14}C determination of oxidation products of OC associated with different sediment grain size fractions in order to constrain the LTTs of OC along a sediment dispersal pathway in a mobile mud belt. Surface sediment samples were collected from two stations proximal and distal to the Yangtze River mouth in the East China Sea (ECS) that follows a relatively simple and well-studied transport trajectory (Fig. 1). The sediments in the mud belt shown are overwhelmingly derived from the Yangtze River materials (Liu et al., 2006, 2007; Xu et al., 2009; Wang et al., 2016), and this characteristic, together with relatively well-constrained OC sources (terrestrial OM exported from the Yangtze River and marine OM produced in the inner shelf, Deng et al., 2006; Xing et al., 2011; Li et al., 2012, 2014; Hu et al., 2012; Zhu et al., 2013), renders this an ideal setting for assessment of LTTs and associated impacts on OC loss. To minimize interferences from both hydrodynamic sorting and diagenetic aging (t_1) of OC attending lateral transport, we target ^{14}C age contrasts among thermally-resolved OC components associated with specific grain size fractions. We determine both LTTs and corresponding OC loss accompanying sediment movement between the two stations. The changing age distribution and thermograms of OC between coupled grain size fractions provide new insights into dynamical processes during lateral transport over continental margins, with implications for carbon cycling on continental margins.

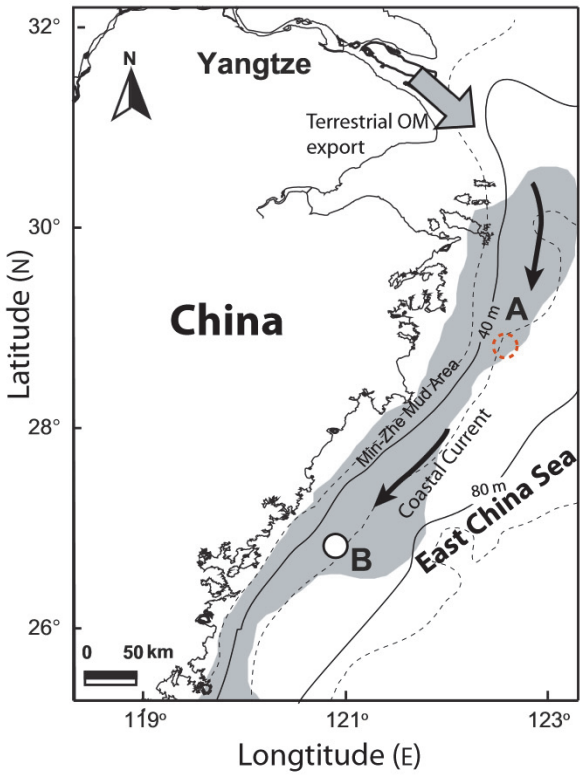

Fig. 1. Sediment core locations (circle with orange dashed outline: location A; circle with black solid outline: location B) and dominant sediment transport trajectory (arrows) on the inner shelf of the ECS. The grey shaded region represents the Min-Zhe mobile mud area (after Xu et al., 2009), and bathymetric contours are based on Lee and Liu (2013). The broad arrow indicates the dominant source of terrestrial sediment and OM (Yangtze river and estuary). (For interpretation of the references to colour in this figure legend, the reader is referred to the web version of this article.)

2. Study area and sampling

This study focuses on a large river-dominated setting on the inner shelf of the ECS, where coastal currents dominate circulation and associated advective processes (Liu et al., 2007) (Fig. 1). Due to a prevailing southward-flowing coastal current, terrestrial materials emanating from the Yangtze River (Liu et al., 2006, 2007; Deng et al., 2006) are largely restricted to the inner shelf of the ECS, leading to the development of an elongated (~800 km) distal subaqueous mud belt extending from near the Yangtze River mouth southwards following the coastline (Liu et al., 2007; Xu et al., 2009). In this shallow region, hydrodynamic processes exert strong influence on the distribution of sedimentary materials, resulting in widespread and intense sediment resuspension (Ono and Guo, 2012; Hung et al., 2013; Pang et al., 2016). Sediments along the mud belt usually experience temporary storage in summer when relatively weak northward currents prevail, and are transported in winter due to strong southward prevailing currents (Yang et al., 2007; Wang et al., 2016; Zhao et al., 2018). Winter storms and associated currents promote sediment resuspension, facilitating southward transport along the mud belt (DeMaster et al., 1985; Milliman et al., 1985; Xu et al., 2012).

Surface sediment (0–2 cm) samples from two sites representing "upstream" (abbr. "location A", 122.58°E, 28.73°N, 63 m water depth) and "downstream" stations (abbr. "location B", 120.83°E, 26.77°N, 47 m water depth), separated by ~275 km on the sediment transport pathway (Fig. 1), were collected using a box corer during cruises of R/V *Dongfanghong II* in July 2013 and October

2011, respectively. Mean grain sizes for both samples are <13 μm, and the percentages of coarser fractions (>63 μm) are <1% by sediment volume. The finer fractions (<20 μm) contain clay minerals and biogenic detritus; whereas the coarse silt fractions (38–63 μm) mostly contain biogenic detritus in this region (Xu et al., 2009). Based on $^{210}Pb_{excess}$ depth profiles, the mixed layer depth in the mudbelt region is ~10 cm (Su and Huh, 2002), and provenance studies based on clay mineralogy (Xu et al., 2009) and terrestrial biomarker distribution (Zhao et al., 2013) indicates that sediments from location B mainly derive from the Yangtze River and upstream regions.

3. Methods

The two surface sediment samples were transferred to the laboratory where they were frozen (−20 °C) and subsequently freeze-dried until further processing. A portion of each sample (~2 g dry weight) was sequentially passed through a cascade of stainless steel sieves using Milli-Q water, yielding the following grain-size fractions: <20 μm (clay and fine silt), 20–32 μm (medium silt), 32–63 μm (coarse silt) fractions. Further details are described in Bao et al. (2018b). Aliquots of freeze-dried grain size fractions were weighed into combusted petri dishes and placed in a desiccator for fumigation (37% HCl, 60 °C, 72 h), followed by subsequent neutralization (NaOH, 60 °C, 72 h) at the National Ocean Science Accelerator Mass Spectrometry (NOSAMS) facility, Woods Hole Oceanographic Institution (WHOI) (Bao et al., 2018c). Blank assessment for the fumigation procedure was performed at NOSAMS (see Supplementary Material for further details). The samples were kept under desiccation until ramped pyrolysis-oxidation (RPO) analysis at NOSAMS (Rosenheim et al., 2008; Bao et al., 2018b,c).

Briefly, RPO analysis involved loading of each sample (~150 mg) into a quartz reactor. The sample was then subjected to a linear temperature ramp (5 °C/min) from 170 °C to 915 °C, which induced sequential thermal decomposition of OC in relation to its thermochemical stability. Evolved components were simultaneously oxidized to CO_2 in a stream of ~8% O_2 in He. The resulting thermal evolution (thermogram) profile of CO_2 was determined using a flow-through infrared CO_2 analyzer. The CO_2 evolved from volatilized components was integrated over five temperature windows, T_1, T_2, T_3, T_4, and T_5, corresponding to 170–320 °C, 320–391 °C, 391–486 °C, 486–570 °C, 570–915 °C, respectively (Fig. 2a). The temperature window of T_5 thermal fraction of 32–63 μm fraction at location A was narrower in range (570–809 °C) due to a gas flow blockage at 809 °C. Evolved CO_2 from each thermal window was cryogenically purified, trapped, and sealed in pyrex tubes for ^{14}C analysis. Tubes were subsequently combusted (525 °C, 1 h) as a final gas purification step prior to ^{14}C measurement (Bao et al., 2018c). The ^{14}C contents were measured using a MICADAS accelerator mass spectrometer (AMS) system at ETH Zurich (Ruff et al., 2007). Radiocarbon data are reported as Fraction modern (Fm) and conventional ^{14}C age (yr BP) as defined by Donahue et al. (1990) and Stuiver and Polach (1977).

4. Results

The RPO thermograms reveal that OC in the different grain size fractions is heterogeneous in terms of thermochemical reactivity. Evolved CO_2 yields, normalized by sample weight, initially increase with increasing temperature (Fig. 2a), reaching a maximum at ~420 °C (T_3) before decreasing and returning to background levels above 915 °C. The three grain size fractions from each location display similar thermograms, however corresponding CO_2 yields (normalized to sample mass) at location B are markedly lower than those at location A (Fig. 2a). ^{14}C ages of CO_2 evolved in the different thermal windows increase with increasing temperature, with a large range in ages between the lowest (T_1, 931–2361 ^{14}C yr BP) and highest (T_5, 8426–12393 ^{14}C yr BP) temperature windows (Fig. 2b, Table 1). Overall, ^{14}C ages of thermal windows at location B are systematically older than those at location A (Fig. 2b).

5. Discussion

5.1. OC aging along the sediment transport pathway

We find decreases in integrated thermogram areas (CO_2 yields) of corresponding samples from location A and B (shaded area, Fig. 2a). The two sample locations receive similar carbon inputs, including terrestrial OM transported from the Yangtze River (Deng et al., 2006; Xing et al., 2011; Li et al., 2012, 2014; Hu et al., 2012; Zhu et al., 2013), as well as marine OM produced in the inner shelf (Xing et al., 2011; Zhao et al., 2018). The discharge of materials derived from the Yangtze River is ~450 Mt/yr, in contrast to ~5 Mt/yr from a local small river (Xu et al., 2009). In addition, the samples were collected from the mud belt that is characterized by high sedimentation rates (~1.5 cm/yr; Liu et al., 2006; Qiao et al., 2017) and similar mixed layer depths (~10 cm, Su and Huh, 2002) at both locations. The loss in OC (i.e., reduction in CO_2 yields) is thus not considered to be a consequence of differences in *in-situ* OM remineralization at the two locations because of the similar grain size distributions (and hence similar physical protection mechanisms) of corresponding sub-fractions from the two locations, implying that degradation of OC occurred along the dispersal pathway (Aller and Blair, 2004; Aller et al., 2008; Liu et al., 2006; Bao et al., 2016, 2019).

We observe shifts in ^{14}C ages for the corresponding thermal windows (T_1 to T_5) between locations A and B (Fig. 2, Table 1), suggesting that net aging of sedimentary OC occurred during translocation along the ~275 km transport pathway. Given the relatively shallow oxygen penetration depths (typically only a few mm) in such coastal muddy areas (Glud, 2008), the observed ^{14}C changes are thus unlikely to result from differences in *in-situ* OET (~1 yr). Additionally, while sediment fluxes from the Yangtze River vary seasonally (Du et al., 2016; Wang et al., 2016), the composition and OC ^{14}C of river suspended particles is relatively uniform ($\Delta^{14}C$: −114 ± 10‰, Wang et al., 2012; Wu et al., 2018). Due to the seasonally-oscillating current trajectories and intensities on the inner shelf of the ECS that result in sediment storage in summer and transport in winter, the net sediment transport is southward along the mud belt (DeMaster et al., 1985; Milliman et al., 1985; Yang et al., 2007; Xu et al., 2012). Given the aforementioned uniformity in source composition, as well as high prevailing sedimentation rates and greater mixed layer depths relative to that of the sediment sampling interval (0–2 cm), we argue that observed age differences among grain sizes and thermal fractions between the two locations are unlikely to reflect seasonal variability in OC characteristics or bioturbation processes. In addition, there is no evidence to support additional inputs of pre-aged OC at location B compared to the overwhelming southward supply of Yangtze River-derived materials. According to mineralogical and modeling analyses, pre-aged OC originating from Taiwan island would only exert local influence outside of the mudbelt (i.e., southern ECS and western Taiwan Strait, Xu et al., 2009, 2012; van der Voort et al., 2018; Bao et al., 2018d). We therefore conclude that the differences in ^{14}C ages primarily reflect "diagenetic aging" resulted from losses of OC content (t_1) coupled with "transport time-associated aging" (t_2) of OC as a result of translocation from location A to B along the mud belt (Figs. 1 and 2).

During transport from location A to B, the magnitude of change in ^{14}C age and CO_2 yield differs between corresponding thermal

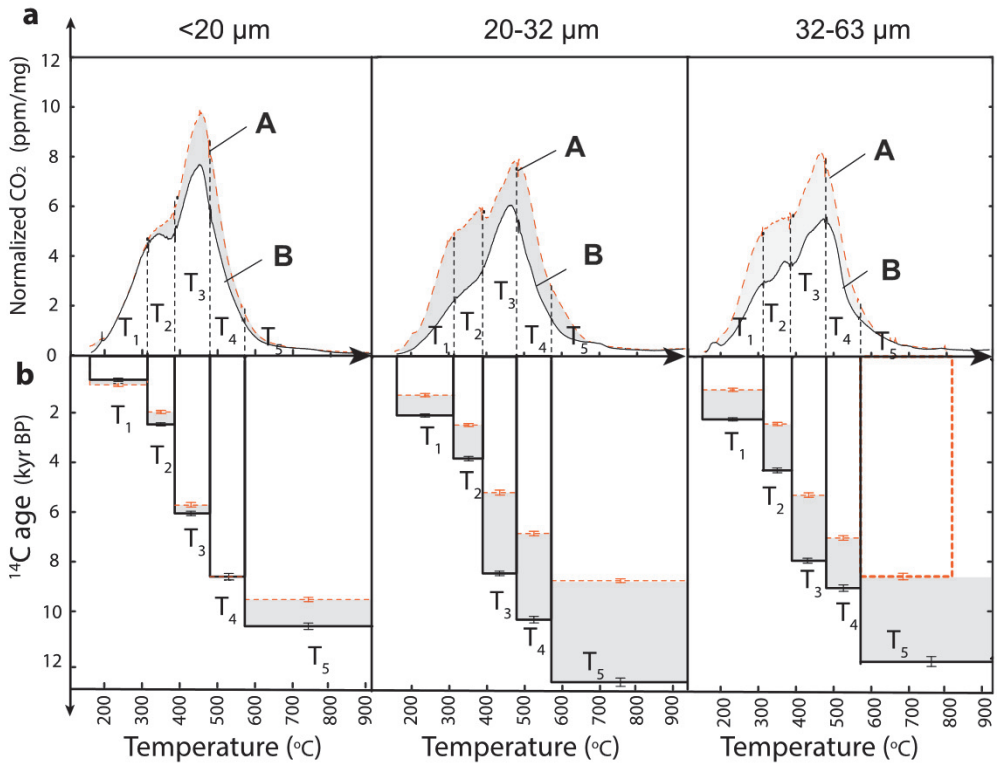

Fig. 2. (a) The CO_2 thermograms of the three grain size fractions (<20 μm, 20–32 μm, 32–63† μm) from location A (dashed and orange line) and B (solid black line) are normalized by weights of samples (ppm/mg). The grey shaded area highlights OC loss; (b) conventional radiocarbon ages (yr BP) of discrete thermal components (T_1–T_5) for each grain size fraction. †The temperature range of the T_5 thermal fraction for 32–63 μm at location A is 570–809 °C. (For interpretation of the references to colour in this figure legend, the reader is referred to the web version of this article.)

Table 1
^{14}C ages and Fm values of CO_2 released from thermal decomposition windows for grain size fractions at location A and B.

	Thermal decomposition Fraction 1 (170–320 °C)		Thermal decomposition Fraction 2 (320–391 °C)		Thermal decomposition Fraction 3 (391–484 °C)		Thermal decomposition Fraction 4 (484–570 °C)		Thermal decomposition Fraction 5 (570–915 °C)†	
Grain size fraction (μm)		Fm		Fm		Fm		Fm		Fm
	Age (^{14}C yr)		Age (^{14}C yr)		Age (^{14}C yr)		Age (^{14}C yr)		Age (^{14}C yr)	
A Station										
<20	1117 ± 85	0.8701	2000 ± 84	0.7796	5861 ± 97	0.4821	8852 ± 101	0.3322	9549 ± 103	0.3046
20–32	1324 ± 77	0.8481	2324 ± 81	0.7487	5262 ± 91	0.5194	6923 ± 96	0.4224	8860 ± 100	0.3319
32–63	1229 ± 86	0.8581	2470 ± 86	0.7352	5280 ± 107	0.5182	7040 ± 111	0.4163	8426 ± 123	0.3503
B Station										
< 20	931 ± 86	0.8906	2621 ± 90	0.7216	6080 ± 103	0.4691	8792 ± 132	0.3347	10582 ± 136	0.2679
20–32	2172 ± 85	0.7631	3858 ± 91	0.6186	8515 ± 120	0.3464	10374 ± 141	0.2749	12393 ± 160	0.2138
32–63	2361 ± 84	0.7454	4341 ± 101	0.5825	7990 ± 123	0.3699	9105 ± 140	0.3219	11892 ± 169	0.2276

Note: †The temperature range of the T_5 thermal fraction for the Station A 32–63 μm sample was 570–809 °C.

windows. Taking the 20–32 μm fractions as an example, the ^{14}C age change of T_3 windows is comparable to those of T_5 windows (3252 ± 211 yr and 3533 ± 260 yr for T_3 and T_5 fractions, respectively, Table 1), whereas the corresponding decrease in yield for the former is less than for the latter thermal window (CO_2 yield changes: 14% and 31%, respectively; Fig. 2). This decoupling of changes in ^{14}C age and OC content among thermal fractions suggests that selective diagenetic aging occurs during the transport process. Selective degradation of younger, more labile OC (that tends to decompose at lower temperatures and thus manifest itself in CO_2 evolved in the lower temperature windows, Capel et al., 2005, 2006; Bao et al., 2018c) leads to diagenetic aging (t_1), contributing to a net shift in ^{14}C age. The magnitude of t_1 depends on the proportional change in younger (labile) and older (refractory) OC during transport. In addition, the ^{14}C age of T_1 fraction in the <20 μm fractions at location B are younger than the corresponding fraction from location A. This reflects either (*i*) the addition of younger OM to the abundant mineral surfaces in this fine grain size fraction during lateral transport from location A to B (which we consider the most probable scenario), and/or (*ii*) the degradation of relatively-old OC in the lower temperature thermal components (which is considered less probable). The OC loss is likely a function of both OM reactivity including physical protection of mineral surfaces depending on grain size (Bao et al.,

2018d). Since sediment grain size is linked to the extent of degradation of OC (Bao et al., 2016, 2019), it is difficult to distinguish varying degradation of OM as resulting from exposure to oxidative conditions versus those related to timescale of lateral transport (Keil et al., 2004; Bröder et al., 2018). As the distance between the two locations is fixed, variation in LTTs among different grain size fractions emerges as a critical factor that influences timescales of exposure to oxidative conditions during translocation of sedimentary OM.

5.2. Estimation of LTTs using RPO and ^{14}C measurements

In order to estimate LTTs, we compare ^{14}C contents (Fm values) of corresponding thermal windows from location A and B (Fig. 3a). The strong linear relationships ($R^2 = 0.98$) among all the thermal components of grain size fractions suggest that ^{14}C results of any coupled-thermal fractions (T_n) would follow the regression lines (Fig. 3a). We assume that all grain size fractions from both location A and B contain a component of refractory, fossil (i.e., ^{14}C-dead) OC derived from sedimentary rock erosion, and that this is entrained in the suspended load exported from the Yangtze River. Indeed, there is direct evidence for the accumulation of fossil OC in inner shelf sediments of the ECS (Huang et al., 2015). Such refractory carbon would mostly decompose at higher temperatures, and for the purpose of this discussion we define this fossil OC as thermal fraction "T_x". Given its fossil character, this thermal fraction should fall on the same regression lines, and would theoretically plot at the intercept (Fm = 0) for both location A and B (Fig. 3b). Given that Fm values of any coupled-thermal fractions should follow the regression lines, this would imply a downward shift in this linear regression line for each thermal window. Taking the 20–32 μm fractions as an example, this is indicated by a shift in slope (i.e., from the red line to the dashed line in Fig. 3b), and assumes that the existence of thermal fractions exclusively reflecting ^{14}C-dead OC could be identified and measured.

Next, we utilize constraints from radioactive isotope (^{14}C) decay to derive transport times. The equation governing radioactive decay (t) is:

$$N_B = N_A e^{(-\lambda t)} \quad (1)$$

where N_A is the number of atoms of the radioactive isotope in sample A, and N_B is the number of atoms left after time t (Stuiver and Polach, 1977). λ is the "true" decay constant for radiocarbon: 0.000121, and Fm is R_{sample}/R_{modern}, where R_{sample} is $^{14}C/^{12}C$ ratio for the sample and R_{modern} is $^{14}C/^{12}C$ ratio for isotopic fractionation-normalized standard in the year 1950. In our case, LTT indicates radiocarbon decay during the transport, i.e., $t = t_2$, leading from Eq. (1) to the following expression:

$$Fm_B = Fm_A e(-\lambda t_2) \quad (2)$$

where Fm_A, Fm_B are Fm values of corresponding organic components from locations A and B, respectively. Since thermal fractions from both locations correspond to the same temperature windows, Fm_A, Fm_B are used to compare changes in ^{14}C content between the two locations. Eq. (2) can thus be rewritten as:

$$t_2 = 8267 \times ln(Fm_A/Fm_B) \quad (3)$$

Thus, t_2 can be calculated through Eq. (3) if Fm_A/Fm_B is given. Taking the 20–32 μm grain size fraction as an example once again, Fig. 3b shows the corresponding relationship between Fm values of the different thermal components. In Fig. 3b, Fm_A/Fm_B for each thermal window corresponds to the slope of the linear regression when the regression line passes through Fm = 0. Since the existence of higher temperature thermal windows (i.e., $Tn > T_5$) will increase the slope of this regression line (Fig. 3b), consequently, the line joining the data point for the highest temperature window (i.e., T_5) and Fm = 0 has the smallest slope (Fig. 3b), and hence yields minimum values for t_2 (LTT) according to Eq. (3). Based on these relationships, given that the sample at "downstream" location B must be transported from the "upstream" location A, we calculate minimum estimated LTTs among the different grain size fractions between two locations as 1060 ± 240 yr, 3640 ± 270 yr, and 3570 ± 300 yr for the <20, 20–32, and 32–63 μm grain size fractions, respectively. Due to incomplete collection of T_5 fraction in 32–63 μm fraction from the location A sample (see Section 3; Fig. 2b) and anticipation that the CO_2 evolved at higher temperatures (>809 °C) would carry a more ^{14}C-depleted signature (Bao et al., 2018c), the measured Fm value for component T_5 at location A may be higher than actual value, leading to artificially high corresponding t_2 for this fraction.

In highly energetic regions such as mobile mud belts, protracted particle transport occurs as a consequence of entrainment in repeated deposition-resuspension loops along the seabed. The mean residence time of particles within the benthic nepheloid layer (BNL) prior to deposition has been estimated to be on the order of years (McCave, 2009), however such particles may undergo many episodes of re-emplacement in the BNL before permanent sedimentation and burial (McKee et al., 1983). The large observed LTTs are attributed to this process of repeated deposition-resuspension, punctuated by periodic residence on the seafloor during transit along the dispersal pathway. Moreover, as the study area is characterized by seasonally-oscillating southward- and northward-flowing currents (Chen, 2009), this bi-directional flow serves to prolong the transport time of sedimentary OM. We infer that the longer LTT for the 20–32 μm grain size fraction reflects the greater propensity of this fraction to undergo resuspension and mobilization relative to the other grain size fractions (Bao et al., 2016). The variation in LTTs among different grain size sediments on the inner shelf of the ECS, and a longer LTT of the 20–32 μm fraction compared with other grain size sediments (20–32 μm: ~13 yr/km, <20 μm fraction: ~4 yr/km), are consistent with the recent study for estimation of LTTs in the Bohai-Yellow Sea region using compound-specific radiocarbon analysis on different grain size fractions of surface sediments (20–32 μm, ~3 yr/km; <20 μm fraction, ~0.5 yr/km; Bao et al., 2018a).

5.3. Relationship between loss and aging of OC

Although the present findings are based on measurements of a limited number of thermal windows for selected grain size fractions of sediments recovered at only two locations, they serve to highlight the potential of this novel analytical approach as a means to assess the influence of LTTs on OC degradation and carbon cycling in shallow marginal sea systems. Due to their varying propensities for mobilization, different grain size fractions and associated OC vary in net transport speed over the same travel distance (ranging from 259 ± 48 m/yr to 76 ± 5 m/yr for <20 μm and 20–32 μm fractions, respectively, along the 275 km-long transit between location A and B). Furthermore, these grain size-specific differences in LTTs may, in turn, affect OETs and thus sedimentary OC contents (Table 2). As previously discussed, decreased CO_2 yields between samples from location A and B likely reflect OC loss (shaded thermogram area, Fig. 2). Combined with available data of total organic carbon contents (TOC) of grain size fractions (Bao et al., 2016), we assess offsets as loss of OC between corresponding grain size fractions. The ratios of offset to original TOC, as defined by values for upstream location A and calculated as OC loss % (Table 2), suggest an apparent relationship between OC loss % and LTT (Fig. 4). Greater OC loss at longer LTTs implies that protracted lateral transport prolongs exposure to oxygenated bottom waters (i.e., longer OET; Hartnett et al., 1998) and enhances OC

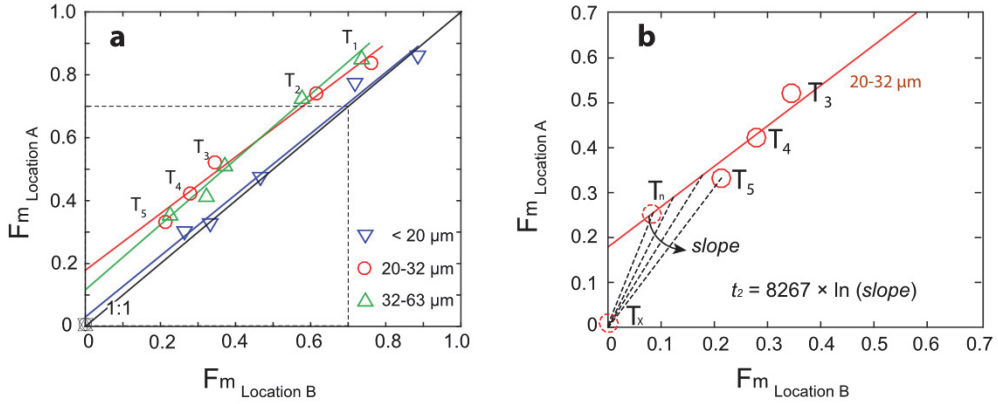

Fig. 3. (a) Cross-plot of (and corresponding regression lines for) Fm values of thermal components (T_1-T_5) for individual grain size fractions from location A versus B. Assuming that there is no offset due to aging processes, corresponding thermal components would plot on a 1:1 (black) line; (b) fractions as an expanded plot (see dashed box in Fig. 3a), taking the 20–32 μm grain size fraction as an example, showing the relationship between Fm values of thermal components. In this case, regression lines are forced through Fm = 0 (dashed lines), representing extrapolation to a high temperature (most refractory and therefore ^{14}C-dead) thermal component. T_n represents any coupled-thermal fractions. Incorporation of the resulting values for slopes of the regression into Eq. (3) yields LTTs for OM associated with specific grain size fractions along the transport pathway.

Table 2
Total organic carbon contents, CO_2 yields, and OC loss % of grain size fractions for A and B locations.

Locations	TOC* (%)	ΣCO_2 yield§ (ppm/mg)	Average
<20 μm at A	0.80	2000	
<20 μm at B	0.75	1717	
Offset	0.05	283	
Loss OC %	6.3	14.2	10.3 ± 5.6
20–32 μm at A	0.95	1960	
20–32 μm at B	0.49	1248	
Offset	0.46	712	
Loss OC %	48.4	36.3	42.4 ± 8.6
32–63 μm at A	0.97	1984#	
32–63 μm at B	0.62	1310	
Offset	0.35	674	
Loss OC %	36.1	34.0	35.0 ± 1.5

Note: OC loss % is derived from two approaches: (i) the ratio of measured TOC % offset between location A and B to TOC % at location A; (ii) the ratio of ΣCO_2 yield offset between A and B location to ΣCO_2 yield of A location.

The temperature range is from 170 to 809 °C.

* The data of total organic carbon contents (TOC, ±0.1[SD] %) is cited from Bao et al. (2016).

§ ΣCO_2 yield is summary of CO_2 concentration at each temperature ranging from 170 to 915 °C divided by loaded sample's weight.

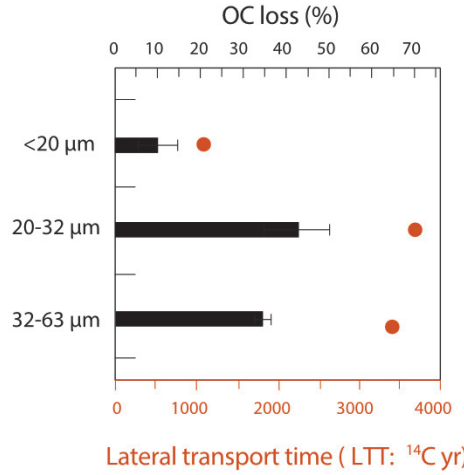

Fig. 4. Estimated extent of OC loss (%; histograms) as a function of the lateral transport time (LTT; solid circles) for OM residing in different grain size fractions.

degradation prior to eventual burial. While Keil et al. (2004) considered that the influence of this transport-associated *t*OET is unrelated to OC source and history, we suggest that the degradation is selective as a consequence of varying hydrodynamic properties as a function of sediment grain size.

The above estimates are based on the straight-line distance between two locations. However, reworking and redistribution of sediments *within* the mud belt would result in greater overall transport distance, and thus the above-calculated transport speeds could be considered as a minimum. Nevertheless, the net effect of sediment redistribution processes is an overall aging of OC in "downstream" locations (Fig. 2b). These processes might also help to explain older ^{14}C ages of foraminifers in the southern mud belt than those from the same sediment layer in the northern mud belt (Liu et al., 2007). Additionally, the net north-to-south direction of prevailing currents both constrain sediment source in the mud belt and limit escape of terrigenous materials discharged from the Yangtze River to the outer-shelf and deep ocean (Liu et al., 2007; Xu et al., 2009). Such mobile mud belts are found on other river-dominated margins (Gordon et al., 2001; McKee et al., 2004; Aller, 1998), where entrained terrestrial OM would anticipate experience similar aging as a function during translocation. Upon export to the ocean, terrestrial OM is subject to remobilization and redistribution regardless of whether it accumulates in mud belts. Many lines of evidence indicate that aging of OM due to lateral sediment redistribution is a widespread phenomenon on continental margins (e.g., Southern Chile, Namibian margin, northwest African margin, southern Adriatic Sea, Gulf of Lions, Bao et al., 2018d and reference therein), and even in the deep ocean (Hwang et al., 2010, Bao et al., 2018e). Given that the magnitude (timescale) of OC aging (LTTs), which depends on specific hydrodynamic conditions (Bao et al., 2019), emerges as an important factor controlling on preservation and degradation of the corresponding sedimentary OM, further investigations are needed to establish quantitative relationships between LTTs and OC degradation for accurate estimation of impacts on sedimentary OC burial and flux on continental margins.

6. Conclusions

We describe an approach involving combined RPO and ^{14}C analysis applied to discrete grain size fractions in order to constrain lateral transport times (LTTs) of OC on continental shelves, applying it to sediments from two stations separated by ~275 km along a mud

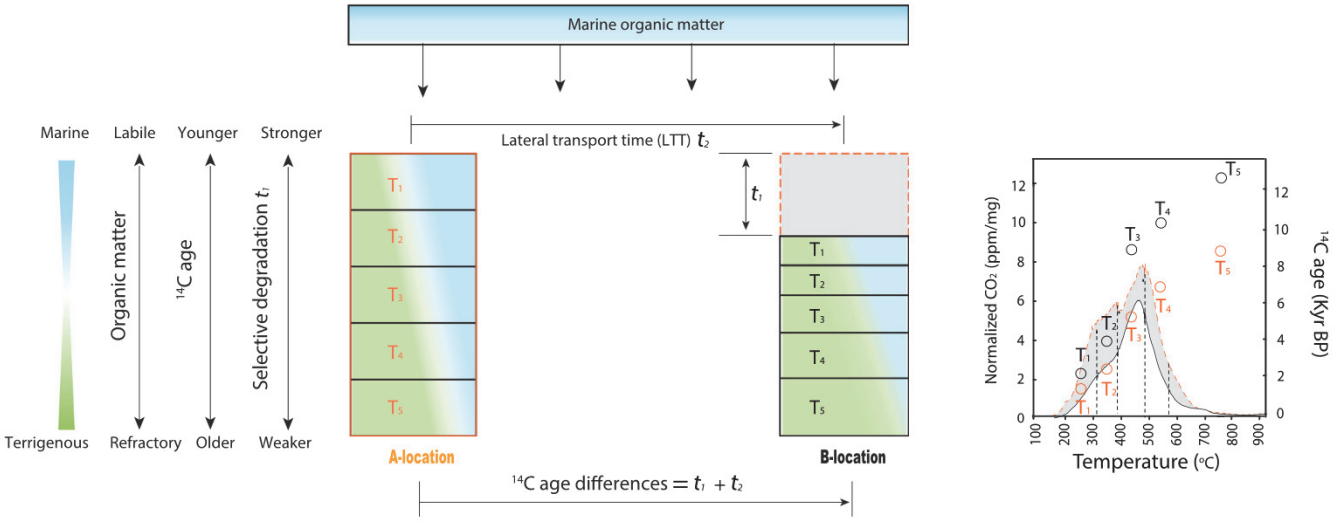

Fig. 5. Conceptual framework that depicts the relationship between t_1, and t_2, and corresponding influences on ^{14}C composition in relation to OC degradation. The sizes of T_n boxes represent the corresponding OC%. Orange dashed box represents the OC loss. Top box and arrows show potential marine OM continuously influencing sedimentary OM along a lateral transect. Taking the 20–32 μm grain size fraction as an example in the right plot, it shows mass-normalized (ppm/mg) CO_2 thermograms of upstream (dashed and orange line) and downstream (solid and black line) samples. Right Y axis shows the ^{14}C age of thermal windows (upstream sample: orange circles; downstream sample: black circle). (For interpretation of the references to colour in this figure legend, the reader is referred to the web version of this article.)

belt on the inner shelf of the ECS. Lateral transport results in an apparent net "aging" of residual OC as a consequence of both diagenetic processes (t_1) and LTTs (t_2) associated with sediment translocation (Fig. 5). The former (t_1) manifests itself in shifts in the RPO thermograms of grain size fractions between the two locations, as well as corresponding increases in the overall age of residual OC. Constraints on t_2 (LTT) of the associated OC are provided using ^{14}C age differences for higher temperature (i.e., more chemically refractory) organic components within specific grain size fractions. Calculated LTTs between the two locations vary between ~3640 and 1060 yr for OC associated with the medium silt (20–32 μm) and clay and fine silt (<20 μm) grain size sediment fractions, respectively (corresponding to average transport velocities of ~79 and 259 m/yr, respectively). Furthermore, a correspondence between the extent of OC loss and LTTs highlights the influence of the latter on the fate of OM. While further work is required to develop robust temporal constraints and to elucidate underlying processes, our findings suggest that timescales for lateral transport of OC within mud belts are substantial (centuries to millennia), and can trigger significant OM remineralization and apparent aging of residual OM. The extent of these processes likely depends on multiple factors (e.g., length- and time-scale of transport, oxygen availability) but requires consideration in the context of carbon-cycling and OC burial on continental shelves, as well as for interpretation of sedimentary records.

Acknowledgements

This study was supported by Doc. Mobility fellowship (No. P1EZP2_159064, R.B.) from the Swiss National Science Foundation (SNSF), the SNSF "CAPS-LOCK" project 200021_140850 (T.I.E.), the National Natural Science Foundation of China (No. 41520104009 and 41630966, M.Z.) and the "111" project (B13030). We thank the support of the NOSAMS staff in the execution of this project. We appreciate the assistance from members of the Laboratory for Ion Beam Physics in all aspects of the AMS measurements. We appreciate the suggestions from Prof. Robert Aller (Stony Brook University) on earlier drafts of the manuscript. We thank two anonymous reviewers for providing helpful comments on the manuscript.

Appendix A. Supplementary material

Supplementary data to this article can be found online at https://doi.org/10.1016/j.orggeochem.2019.01.007.

Associate Editor—**Marcus Elvert**

References

Aller, R.C., 1998. Mobile deltaic and continental shelf muds as suboxic, fluidized bed reactors. Marrine Chemistry 61, 143–155.
Aller, R.C., Blair, N.E., 2004. Early diagenetic remineralization of sedimentary organic C in the Gulf of Papua deltaic complex (Papua New Guinea): net loss of terrestrial C and diagenetic fractionation of C isotopes. Geochimica et Cosmochimica Acta 68, 1815–1825.
Aller, R.C., Blair, N.E., Brunskill, G.J., 2008. Early diagenetic cycling, incineration, and burial of sedimentary organic C in the central Gulf of Papua (Papua New Guinea). Journal of Geophysical Research 113, F01S09. https://doi.org/10.1029/2006JF000689.
Bao, R., McIntyre, C., Zhao, M., Zhu, C., Kao, S., Eglinton, T.I., 2016. Widespread dispersal and aging of organic carbon in shallow marginal seas. Geology. https://doi.org/10.1130/G37948.1.
Bao, R., Uchida, M., Zhao, M., Haghipour, N., Montlucon, D., MiNichol, A., Wacker, L., Hayes, J.M. Eglinton T.I., 2018a. Organic carbon aging during cross-shelf transport. Geophysical Research Letters https://doi.org/10.1029/2018GL078904.
Bao, R., McNichol, A.P., McIntyre, C.P., Xu, L., Eglinton, T.I., 2018b. Dimensions of radiocarbon variability within sedimentary organic matter. Radiocarbon 60, 775–790.
Bao, R., McNichol, A.P., Hemingway, J., Lardie, M., Eglinton, T.I., 2018c. Influence of different acid treatments on the radiocarbon content spectrum of sedimentary organic matter determined by RPO/Accelerator Mass Spectrometry. Radiocarbon 1–15. https://doi.org/10.1017/RDC.2018.125.
Bao, R., van der Voort, T.S., Zhao, M., Guo, X., Montluçon, D., McIntyre, C., Eglinton, T. I., 2018d. Influence of hydrodynamic processes on the fate of sedimentary organic matter on continental margins. Global Biogeochemical Cycles 32. https://doi.org/10.1029/2018GB005921.
Bao, R., Strasser, M., McNichol, A.P., Haghipour, N., McIntyre, C., Wefer, G., Eglinton, T.I., 2018e. Tectonically-triggered sediment and carbon export to the Hadal zone. Nature Communications 9. https://doi.org/10.1038/s41467-017-02504-1.
Bao, R., Blattmann, T.M., McIntyre, C., Zhao, M., Eglinton, T.I., 2019. Relationships between grain size and organic carbon ^{14}C heterogeneity in continental margin sediments. Earth and Planetary Science Letters 505, 76–85.
Bröder, L., Tesi, T., Andersson, A., Semiletov, I., Gustafsson, Ö., 2018. Bounding cross-shelf transport time and degradation in Siberian-Arctic land-ocean carbon transfer. Nature Communications. https://doi.org/10.1038/s41467-018-03192-1.
Capel, E.L., Bol, R., Manning, D., 2005. Application of simultaneous thermal analysis mass spectrometry and stable carbon isotope analysis in a carbon sequestration

study. Rapid Communnication Mass Spectrometry 19, 3192–3198. https://doi.org/10.1002/rcm.2145.
Capel, E.L., de la Rosa Arranz, J.M., González-Vila, F.J., González-Perez, J.A., Manning, D.A., 2006. Elucidation of different forms of organic carbon in marine sediments from the Atlantic coast of Spain using thermal analysis coupled to isotope ratio and quadrupole mass spectrometry. Organic Geochemistry 37, 1983–1994.
Chen, C.-T.A., 2009. Chemical and physical fronts int eh Bohai, Yellow and East China Sea. Journal of Marine System 78, 394–410.
DeMaster, D.J., McKee, B.A., Nittrouer, C.A., Jiangchu, Q., Guodong, C., 1985. Rates of sediment accumulation and particle reworking based on radiochemical measurements from continental shelf deposits in the East China Sea. Continental Shelf Research 4, 143–158.
Deng, B., Zhang, J., Wu, Y., 2006. Recent sediment accumulation and carbon burial in the East China Sea. Global Biogeochemistry Cycles 20. https://doi.org/10.1029/2005GB002559.
Donahue, D.J., Linick, T.W., Jull, A., 1990. Isotope-ratio and background corrections for accelerator mass spectrometry radiocarbon measurements. Radiocarbon 32, 135–142.
Du, J., Du, J., Huang, D., Wang, J., Zhang, J., 2016. Seasonal distribution patterns of ^{7}Be and ^{210}Pb in surface sediments in the Changjiang Estuary, China and their implication. Journal of Marine Systems 154, 41–49.
Gordon, E.S., Goni, M.A., Roberts, Q.N., Kinke, G.C., Allison, M.A., 2001. Organic matter distribution and accumulation on the inner Louisiana shelf west of the Atchafalaya River. Coninental Shelf Research 21, 1691–1721.
Glud, R.N., 2008. Oxygen dynamics of marine sediments. Marine Biology Research 4, 243–289. https://doi.org/10.1080/17451000801888726.
Hartnett, H.E., Keil, R.G., Hedges, J.I., Devol, A.H., 1998. Influence of oxygen exposure time on organic carbon preservation in continental margin sediments. Nature 391, 572–575. https://doi.org/10.1038/35351.
Hedges, J.I., Hu, F.S., Devol, A.H., Hartnett, H.E., Tsamakis, E., Keil, R.G., 1999. Sedimentary organic matter preservation; a test for selective degradation under oxic conditions. American Journal of Science 299, 529–555.
Hu, L., Shi, X., Yu, Z., Lin, T., Wang, H., Ma, D., Guo, Z., Yang, Z., 2012. Distribution of sedimentary organic matter in estuarine–inner shelf regions of the East China Sea: implications for hydrodynamic forces and anthropogenic impact. Marine Chemistry 142, 29–40.
Huang, L., Zhang, J., Wu, Y., Wang, J., 2015. Distribution and preservation of black carbon in the East China Sea sediments: Perspectives on carbon cycling at continental margins. Deep Sea Research Part II 124, 43–52.
Hung, C.C., Tseng, C.W., Gong, G.C., Chen, K.S., Chen, M.H., Hsu, S.C., 2013. Fluxes of particulate organic carbon in the East China Sea in summer. Biogeosciences 10, 6469–6484.
Hwang, J., Druffel, E.R., Eglinton, T.I., 2010. Widespread influence of resuspended sediments on oceanic particulate organic carbon: Insights from radiocarbon and aluminum contents in sinking particles. Global Biogeochemical Cycles 24. https://doi.org/10.1029/2010GB003802.
Inthorn, M., Wagner, T., Scheeder, G., Zabel, M., 2006. Lateral transport controls distribution, quality, and burial of organic matter along continental slopes in high-productivity areas. Geology 34, 205–208.
Keil, R.G., Dickens, A.F., Arnarson, T., Nunn, B.L., Devol, A.H., 2004. What is the oxygen exposure time of laterally transported organic matter along the Washington margin? Marine Chemistry 92, 157–165.
Li, X., Bianchi, T.S., Allison, M.A., Chapman, P., Mitra, S., Zhang, Z., Yang, G., Yu, Z., 2012. Composition, abundance and age of total organic carbon in surface sediments from the inner shelf of the East China Sea. Marine Chemistry 145, 37–52.
Li, D., Yao, P., Bianchi, T.S., Zhang, T., Zhao, B., Pan, H., Wang, J., Yu, Z., 2014. Organic carbon cycling in sediments of the Changjiang Estuary and adjacent shelf: Implication for the influence of Three Gorges Dam. Journal of Marine Systems 139, 409–419.
Liu, J., Li, A., Xu, K., Velozzi, D., Yang, Z., Milliman, J., DeMaster, D., 2006. Sedimentary features of the Yangtze River-derived along-shelf clinoform deposit in the East China Sea. Continental Shelf Research 26, 2141–2156.
Liu, J., Xu, K., Li, A., Milliman, J., Velozzi, D., Xiao, S., Yang, Z., 2007. Flux and fate of Yangtze River sediment delivered to the East China Sea. Geomorphology 85, 208–224.
Lee, H.-J., Liu, K.-K., 2013. Tidal effects on Changjiang plume dispersal in the East China Sea. Journal of Marine Science and Technology 21, 342–352. https://doi.10.6119/JMST-013-0207-1.
Mayer, L.M., 1994. Surface area control of organic carbon accumulation in continental shelf sediments. Geochimica et Cosmochimica Acta 58, 1271–1284.
McCave, I.N., 2002. A poisoned chalice? Science 298, 1186–1187.
McCave, I.N., 2009. Nepheloid layers. In: Steele, J.H., Thorpe, S.A., Turekian, K.K. (Eds.), Elements of Physical Oceanography: A derivative of the Encyclopedia of Ocean Sciences. Elsevier, pp. 0–282.
McKee, B.A., Nittrouer, C.A., DeMaster, D.J., 1983. Concepts of sediment deposition and accumulation applied to the continental shelf near the mouth of the Yangtze River. Geology 11, 631–633.
McKee, B., Aller, R., Allison, M., Bianchi, T., Kineke, G., 2004. Transport and transformation of dissolved and particulate materials on continental margins influenced by major rivers: benthic boundary layer and seabed processes. Continental Shelf Research 24, 899–926.
Milliman, J.D., Beardsley, R.C., Zuo-Sheng, Y., Limeburner, R., 1985. Modern Huanghe-derived muds on the outer shelf of the East China Sea: identification and potential transport mechanisms. Continental Shelf Research 4, 175–188.
Mollenhauer, G., Kienast, M., Lamy, F., Meggers, H., Schneider, R.R., Hayes, J.M., Eglinton, T.I., 2005. An evaluation of ^{14}C age relationships between co-occurring foraminifera, alkenones, and total organic carbon in continental margin sediments. Paleoceanography 2. https://doi.org/10.1029/2004pa001103.
Mollenhauer, G., McManus, J.F., Wagner, T., McCave, I.N., Eglinton, T.I., 2011. Radiocarbon and ^{230}Th data reveal rapid redistribution and temporal changes in sediment focussing at a North Atlantic drift. Earth and Planetary Science Letters 30, 373–381.
Ohkouchi, N., Eglinton, T.I., Keigwin, L.D., Hayes, J.M., 2003. Spatial and temporal offsets between proxy records in a sediment drift. Science 298, 1224–1227.
Ono, J., Guo, X., 2012. Modeling of suspended particulate matter in the East China Sea. In: Kawaguchi, M., Misaki, K., Sato, H., Yokokawa, T., Itai, T., Nguyen, T.M., Ono, J., Tanabe, S. (Eds.), Interdisciplinary Studies on Environmental Chemistry–Environmental Pollution and Ecotoxicology, pp. 311–319.
Pang, C., Li, K., Hu, D., 2016. Net accumulation of suspended sediment and its seasonal variability dominated by shelf circulation in the Yellow and East China Seas. Marine Geology 371, 33–43.
Qiao, S., Shi, X., Wang, G., Zhou, L., Hu, B., Hu, L., Yang, G., Liu, Y., Yao, Z., Liu, S., 2017. Sediment accumulation and budget in the Bohai Sea, Yellow Sea and East China Sea. Marine Geology 390, 270–281.
Rosenheim, B.E., Day, M.B., Domack, E., Schrum, H., Benthien, A., Hayes, J.M., 2008. Antarctic sediment chronology by programmed-temperature pyrolysis: Methodology and data treatment. Geochemistry Geophysics Geosystems 9. https://doi.org/10.1029/2007GC001816.
Ruff, M., Wacker, L., Gäggeler, H., Suter, M., Synal, H.-A., Szidat, S., 2007. A gas ion source for radiocarbon measurements at 200 kV. Radiocarbon 49, 307–314.
Stuiver, M., Polach, H.A., 1977. Discussion; reporting of C-14 data. Radiocarbon 19, 355–363.
Su, C.-C., Huh, C.-A., 2002. ^{210}Pb, ^{137}Cs and $^{239,\ 240}$ Pu in East China Sea sediments: sources, pathways and budgets of sediments and radionuclides. Marine Geology 183, 163–178.
Tesi, T., Semiletov, I., Dudarev, O., Andersson, A., Gustafsson, Ö., 2016. Matrix-association effects on hydrodynamic sorting and degradation of terrestrial organic matter during cross-shelf transport in the Laptev and East Siberian shelf seas. Journal of Geophyical Research Biogeosciences 121. https://doi.org/10.1002/2015JG003067.
Thomsen, L., Gust, G., 2000. Sediment erosion thresholds and characteristics of resuspended aggregates on the western European continental margin. Deep Sea Research 47, 1881–1897.
Thomsen, L., McCave, I., 2000. Aggregation processes in the benthic boundary layer at the Celtic Sea continental margin. Deep Sea Research 47, 1389–1404.
van der Voort, T.S., Mannu, U., Blattmann, T.M., Bao, R., Zhao, M., Eglinton, T.I., 2018. Deconvolving the fate of carbon in coastal sediments. Geophysical Research Letters 45. https://doi.org/10.1029/2018GL077009.
Wakeham, S.G., Canuel, E.A., Lerberg, E.J., Mason, P., Sampere, T.P., Bianchi, T.S., 2009. Partitioning of organic matter in continental margin sediments among density fractions. Marine Chemistry 115, 211–225.
Wang, J., Du, J., Baskaran, M., Zhang, J., 2016. Mobile mud dynamics in the East China Sea elucidated using ^{210}Pb, ^{137}Cs, ^{7}Be, and ^{234}Th as tracers. Journal of Geophysical Research: Oceans. https://doi.org/10.1002/2015JC011300.
Wu, Y., Eglinton, T.I., Zhang, J., Montlucon, D.B., 2018. Spatio-temporal variation of the quality, origin and age of particulate organic matter transported by the Yangtze River (Changjiang). Journal of Geophysical Research. Biogeosciences. https://doi.org/10.1029/2017JG004285.
Wang, X., Ma, H., Li, R., Song, Z., Wu, J., 2012. Seasonal fluxes and source variation of organic carbon transported by two major Chinese Rivers: The Yellow River and Changjiang (Yangtze) River. Global Biogeochemical Cycles 26. https://doi.org/10.1029/2011GB004130.
Xing, L., Zhang, H., Yuan, Z., Sun, Y., Zhao, M., 2011. Terrestrial and marine biomarker estimates of organic matter sources and distributions in surface sediments from the East China Sea shelf. Continental Shelf Research 31, 1106–1115.
Xu, K., Milliman, J.D., Li, A., Liu, P., Kao, S.-J., Wan, S., 2009. Yangtze-and Taiwan-derived sediments on the inner shelf of East China Sea. Continental Shelf Research 29, 2240–2256.
Xu, K., Li, A., Liu, J.P., Milliman, J.D., Yang, Z., Liu, C.-S., Kao, S.-J., Wan, S., Xu, F., 2012. Provenance, structure, and formation of the mud wedge along inner continental shelf of the East China Sea: a synthesis of the Yangtze dispersal system. Marine Geology 291, 176–191.
Yang, Z., Lei, K., Guo, Z., Wang, H., 2007. Effect of a winter storm on sediment transport and resuspension in the distal mud area, the East China Sea. Journal of Coastal Research, 310–318.
Zhao, Z.S., Li, H.J., Wang, Y.W., Li, G.L., Cao, Y.L., Zeng, L.X., Lan, J., Wang, T., Jiang, G.J., 2013. Source and migration of short-chain chlorinated paraffins in the coastal East China Sea using multiproxies of marine organic geochemistry. Environmental Science and Technology 47, 5013–5022.
Zhao, B., Yao, P., Bianchi, T.S., Arellano, A.R., Wang, X., Yang, J., Su, R., Wang, J., Xu, Y., Huang, X., Chen, L., Ye, J., Yu, Z., 2018. The remineralization of sedimentary organic carbon in different sedimentary regimes of the Yellow and East China Seas. Chemical Geology 495, 104–117.
Zhu, C., Wagner, T., Talbot, H.M., Weijers, J.W., Pan, J.-M., Pancost, R.D., 2013. Mechanistic controls on diverse fates of terrestrial organic components in the East China Sea. Geochimica et Cosmochimica Acta 117, 129–143.